Draft version October 4, 2021
Typeset using LaTeX **twocolumn** style in AASTeX63

Galaxian Contamination in Galactic Reddening Maps

Peter J. Brown[1,2] and Tate Walker[3]

[1] Department of Physics and Astronomy, Texas A&M University, 4242 TAMU, College Station, TX 77843, USA
[2] George P. and Cynthia Woods Mitchell Institute for Fundamental Physics & Astronomy
[3] Department of Aerospace Engineering, Texas A&M University, 4242 TAMU, College Station, TX 77843, USA

ABSTRACT

Estimating the amount of foreground extinction due to the Milky Way dust along the line of sight is often a first step in determining the luminosity of an object. The amount of Galactic dust inferred by infrared emission maps can be contaminated by infrared light from nearby galaxies. By comparing extinction values at and around the location of nearby galaxies, we compile a list of 95 galaxies which likely contaminate the maps with an excess or improperly-subtracted galaxian infrared emission and tabulate our recommend values for the MW contribution. In addition to M82, which inspired this work, six more sources have an excess visual extinction A_V of at least 0.05 mag greater than our annular values, including M83, NGC1313, NGC6822, NGC918, UGC11501, and UGC11797. M33 is shown to be oversubtracted. NGC88 and the outskirts of NGC4258 are located in gaps in the IRAS imaging. The recommended dust map values for the LMC, SMC, and M31 may also not be correctly returned by some software packages. Accurate reddening estimates are important for measuring stellar and supernova luminosities in these nearby galaxies.

Keywords: dust: general, Milky Way: dust

1. INTRODUCTION

As luminosity is a fundamental property of astrophysical objects, properly correcting for the extinction of light due to dust is important. Accurate luminosities are needed for calculating energy budgets, sizes of objects, and the calibration and use of astrophysical objects as standard candles to measure distances in the universe.

Dust extinction can occur anywhere along the line of sight from an object to the observer, including circumstellar dust, dust in the host galaxy of an object, circumgalactic dust, intergalactic dust, and dust in our own Milky Way galaxy. These multiple components can make a full determination of the extinction complicated, but it is usually assumed that the component of dust extinction arising from the MW is the best understood. The all-sky dust reddening maps of Schlegel et al. (1998), hereafter referred to as SFD98, improved on the earlier HI estimates of Burstein & Heiles (1982) by calibrating the luminosity at 100 μm from the Diffuse InfraRed Background Experiment on the Cosmic Background Explorer (DIRBE/COBE) and the Infrared Astronomical Satellite (IRAS) and converting it into the V-band extinction using the colors of elliptical galaxies. These maps have made it convenient to look up the SFD98 reddening (or the rescaling by Schlafly & Finkbeiner 2011) via the NASA Extragalactic Database (NED[1]; Mazzarella et al. 2001) or other electronic queries without having to understand the data, read the paper, or notice the warnings from NED[2]. Combined with the mean value of R_V=3.1 from Fitzpatrick (1999), one can compute the extinction as a function of wavelength or at the effective wavelength of a filter for a particular source. Such ease, however, often makes it too easy to overlook the details and complications extant in the data set.

Dalcanton et al. (2009) mentioned in a footnote that the SFD98 maps were clearly contaminated by M82, brought to our knowledge through studies of the extinction toward the supernova (SN) 2014J (Foley et al. 2014). Johnson et al. (2009) cautioned about not just the contamination of M81 and M82 but also the highly

Corresponding author: Peter J. Brown
pbrown@physics.tamu.edu

[1] https://ned.ipac.caltech.edu/

[2] https://ned.ipac.caltech.edu/classic/help/faq3.html#3a

variable region nearby. Chiang & Ménard (2019) found that even distant galaxy clusters leave a small imprint on the dust maps. As dust reddening from anywhere has strong consequences in the ultraviolet, the authors were led to ask the question "Which nearby galaxies might be contaminating the dust maps in this same way?"

In this short paper we describe how we searched for examples of contaminating galaxies and give a table of recommended extinction values for the ones we found.

2. ANALYSIS

To detect likely point sources from galaxy contaminants in the dust maps, we searched for excesses in A_V at the center of each galaxy of interest compared to the mean of the values 20′ away in each of the four cardinal directions. We could then individually examine sources which were significantly higher than the mean of the 20′ radius. As a baseline for what a significant excess is, we first looked up the A_V values (via IrsaDust.get_extinction_table in the Astroquery Python package) for 102 random positions in the sky. The central and mean radial values are plotted in Figure 1. As expected, most of the points cluster around the 1:1 line compared to the mean value in the surrounding points, and the scatter is a consistent fraction of the central value (note that both axis are on a log scale). From the random positions, we set one and two sigma limits of 12% and 22% which encompass 68% and 95% of the points, respectively. A few points lie significantly below the 1:1 line due to bright spots in the angular regions.

We queried the A_V values at the location of each of the extragalactic sources in Rice et al. (1988), the 70 brightest of which should already have been removed from the SFD98 maps. For our scientific purposes, we also tabulated the nearby host galaxies used to calibrate the Cepheid-Supernova Ia distance ladder (Riess et al. 2016), the SINGS sample (Kennicutt et al. 2003), and over 700 supernova host galaxies observed by Swift (Brown et al. 2014). We manually examine the fields of all galaxies for which the central position has an A_V of 12% greater than the mean of the points at 20′ and all of the sources from Rice et al. (1988).

For each galaxy above our excess threshold, a square InfraRed Space ATLAS image (based on IRAS imaging) 100 μm image 80′ across was created as well as a plot with the A_V as a function of radius out to 20′ in each of the cardinal directions in steps of 1′. Examples are shown in Figure 2. Both of these were visually examined to assess if the central excess was likely due to the flux of the galaxy, part of a region with highly variable infrared flux from the MW, or both. If the galaxy seemed to contribute to the excess, a radius was determined at which the galaxian contribution dropped below the background level. We then queried the A_V values at 360 locations at that radius. We report the median value and standard deviation of those values in Table 1. For galaxies in a region with a highly-variable foreground MW IR emission, such as a gradient, patchy emission, or artifacts, more sophisticated two-dimensional modeling or cross correlation with other forms of reddening estimates might better sample the contaminated region. Though imperfect, we believe our values to more accurately reflect the true MW reddening at the location of the galaxies than the look up tables used based on Schlegel et al. (1998).

Some sources appear to be partially removed, replacing the pixels with the median value of a nearby annu-

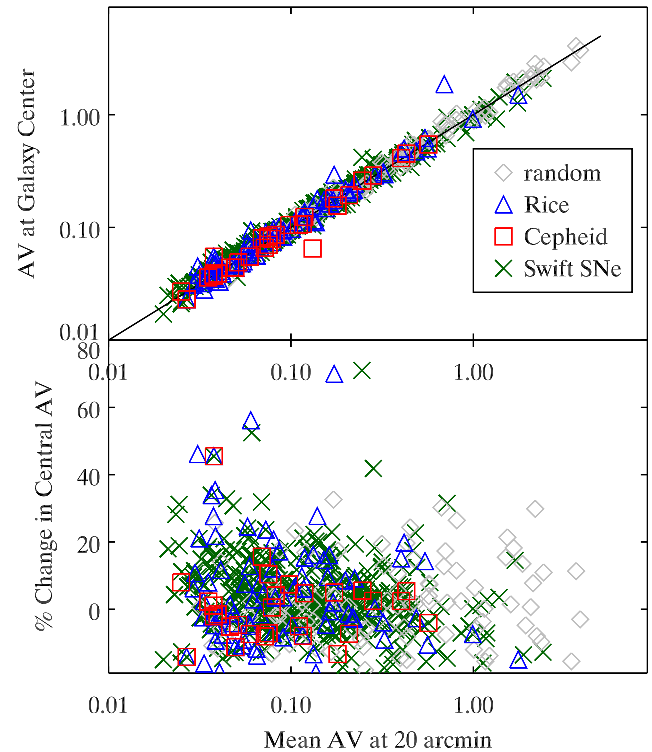

Figure 1. Top panel: The central value of A_V is plotted with respect to the mean of the A_V values 20′ away in each of the four cardinal directions. 102 random positions are plotted in grey. The sample from Rice et al. (1988) which should have already been removed are blue triangles. Nearby galaxies used to calibrate the Cepheid-SN distance ladder (Riess et al. 2016) are plotted as red squares. The sample of Swift supernovae are green crosses. A 1:1 line shows perfect agreement between the values. Bottom panel: A_V differences normalized by the mean A_V at 20′. The fractional difference is fairly constant with A_V. The fractional differences for the random locations have a standard deviation of 12%. This is used as the cutoff for our manual examination.

lus. The replaced region, however, is in some cases too small and the replacement value too bright in the regions passing our cuts. M51 and M83, as shown in Figure 2, are two examples of this. Visual examination of the Rice et al. (1988) galaxies was done to find galaxies with poor subtraction which nevertheless did not meet our criteria of having a significant central excess. M33 is a striking example which appears to be oversubtracted, as shown in 3. In many cases our recommended value is only slightly smaller than the map value ($\sim$0.01 mag), but its use may avoid a small bias. In some instances, such as NGC2442 and NGC4666, our recommended value is close to the replacement value used in the maps. The complexity of the location, however, leads to a higher recommended uncertainty, because the galaxy line of sight may or may not pass through the brighter regions of the foreground emission. Including a higher uncertainty for these objects recognizes that our knowledge of the MW dust is not as complete as is often assumed.

Other values returned from the tools are not properly corrected for the suggested corrections for the nearby Large and Small Magellanic clouds and M31 given in Appendix C of SFD98. The recommended value for the region around M31, for example, is E(B-V)=0.062 (SFD98; 0.055 in the Schlafly & Finkbeiner 2011 system). The Schlafly & Finkbeiner (2011) value of 0.055 is obtained from the NASA Extragalactic Database[3] when searching the position of M31. Since M31 is not removed from the maps, however, one obtains a value of E(B-V)=0.60 (a factor of 10 larger) from the NASA/IPAC Infrared Science Archive from the website[4] or Astroquery in python. This field is shown in the second panel of Figure 3.

Another problematic field we found was in the region of NGC4258. NGC4258 is an important rung of the extragalactic distance scale because of its geometrically-determined distance which is used either as a calibration of or a check of Cepheid distances (Macri et al. 2006; Humphreys et al. 2013; Hoffmann et al. 2016; Reid et al. 2019). There is a clear point source visible in some of the IRAS images. In most of the images available from the NASA/Infrared Processing and Analysis Center (IPAC), however, NGC4258 falls in a gap between data. This results in a discontinuity in the combined images. The central value of A_V derived from the maps is small and appears correct, so analyses using the galaxy value appear fine (e.g. Macri et al. 2006). Using values at the positions of individual objects in the outer fields in the south and east could overestimate the small MW reddening by $\sim 50\%$, as shown in Figure 3. This would be a small effect but potentially significant for objects with low host reddening in a science field where precision and accuracy are critical. NGC88 also falls in a gap. For both of these objects we provide a recommended value within a radius around the galaxy center based on values outside the gap.

Reading the mask values from the SFD data product would catch some of the sources in or near the SMC, LMC, or M31 or for which no IRAS data existed and the COBE/DIRBE maps were used instead. These oversights could just be treated as a bug and corrected in these archives. Since past work may have been incorrectly analyzed, we are publishing this research article as well as notifying the developers in order to promote the best science in past and future analyses.

The list of contaminating galaxies is given in Table 1 with their central coordinates, the radius of contamination, our estimate for A_V, and our estimated uncertainty on A_V. The values for the LMC, SMC and M31 recommended by Appendix C of SFD98 are corrected to the Schlafly & Finkbeiner (2011) system and listed in Table 1 along with the recommended value for M82 from Dalcanton et al. (2009). Thus one could query this table by position in order to update MW reddening values obtained from the IR maps. We note, however, that work requiring precise line of sight extinctions through these large areas should utilize other methods to better constrain the minimum position-dependent line of sight extinction contributed by the Milky Way in these extended areas (e.g. Haschke et al. 2011).

In this paper we have focused on the commonly-used SFD98 maps. Visual inspection of the galaxies flagged in this analysis using the Planck Collaboration et al. (2014) maps reveal the same issues of contamination. The Planck Collaboration et al. (2014) contamination is actually more severe because the extragalactic sources not in the point source catalog were not removed from the IRIS map, while most of the corrections discussed previously were for sources not fully subtracted in SFD98. Our spot checks of significant sources found in SFD are also found in the Planck Collaboration et al. (2014) dustmaps obtained through the dustmaps utility. We recommend that members of the Planck team who understand the data best make a best effort attempt to remove these extragalactic contaminants, possibly using two-dimensional interpolation, power spectra, or gaussian processes to better fill in the contaminated regions than the median-filled circles used here and by SFD. Other methods of reddening determinations, such as stellar colors (Green et al. 2019) and HI maps (Lenz

[3] https://ned.ipac.caltech.edu/

[4] https://irsa.ipac.caltech.edu/frontpage/

et al. 2017), should also be consulted if a precise extinction is needed. Understanding the limitations (such as low HI column density for HI reddening; Lenz et al. 2017) of any method is still important.

Many corrections for extinction already utilize the intrinsic colors of an object (e.g. type Ia supernovae; Phillips et al. 1999) to determine the total reddening to it. An incorrect measure of the MW reddening could be compensated by a larger or smaller value of the host galaxy reddening, yielding the same total extinction if the MW and host galaxy reddening laws are the same. In the limiting case of negligible host reddening the flux could be overcorrected, resulting in bluer colors which might be interpreted as zero or negative reddening depending on the assumed priors in the SN fitting.

3. SUMMARY

In summary, we have searched for galaxies whose infrared emission might significantly contaminate the IRAS images resulting in a overestimate of the foreground MW dust reddening. We provide a table of such galaxies, their coordinates, our recommended values on the Schlafly & Finkbeiner (2011) system, and the radius with which to use replacement values from those looked up by default from the SFD98 maps via NED or Astroquery (Ginsburg et al. 2019). This will be communicated to the developers of such tools, and we make available our code to query our table or the dust maps as appropriate[5]. We recommend, however, that users make themselves aware of the issues of the data they use by reading the original papers even when the data products are made easily accessible via automated sources.

ACKNOWLEDGMENTS

We appreciate useful discussions with D. Schlegel and D. Finkbeiner about the SFD98 maps and comments on the manuscript from N. Suntzeff. Most of this work was done as a student project as part of Texas A&M's Aggie Research Program. This work was also supported by the Mitchell Institute for Fundamental Physics and Astronomy and NASA grant 80NSSC20K0456.

[5] https://github.com/pbrown801/AV
https://zenodo.org/badge/latestdoi/166308993

Facilities: (IRAS)

Software: astropy (Astropy Collaboration et al. 2013; Price-Whelan et al. 2018), astroquery (Ginsburg et al. 2019), scipy (Jones et al. 2001–; Virtanen et al. 2020)

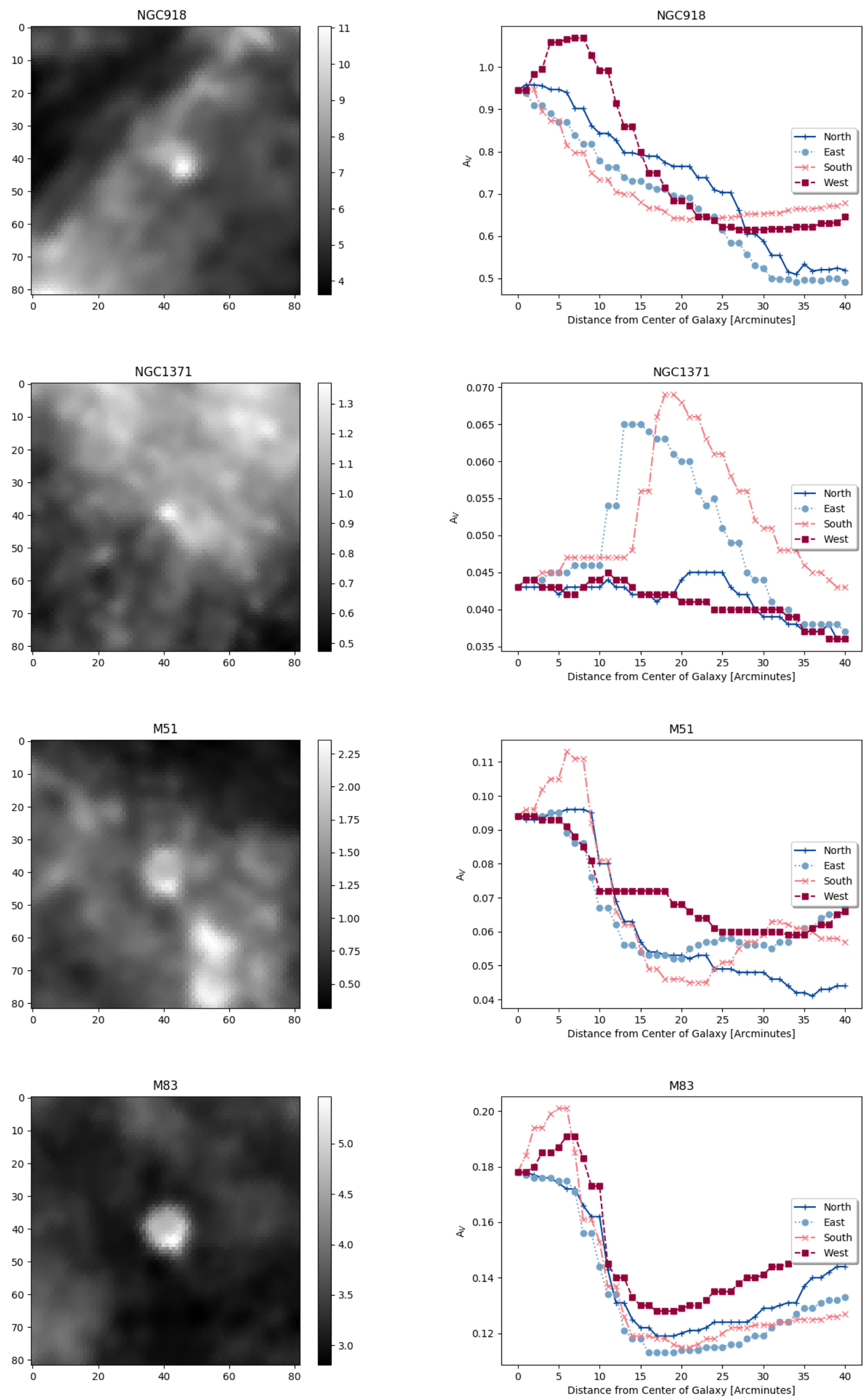

Figure 2. 100 μmIRAS images ($80' \times 80'$with North pointing up) on the left and the corresponding plots of A_V v. distance from center for a few galaxies illustrating the range of contamination. The top panel shows the small but clear contribution of NGC1371. The second panel shows the more complicated field of NGC1448. The bottom two panels show the uncomplete subtraction of M51 and M83.

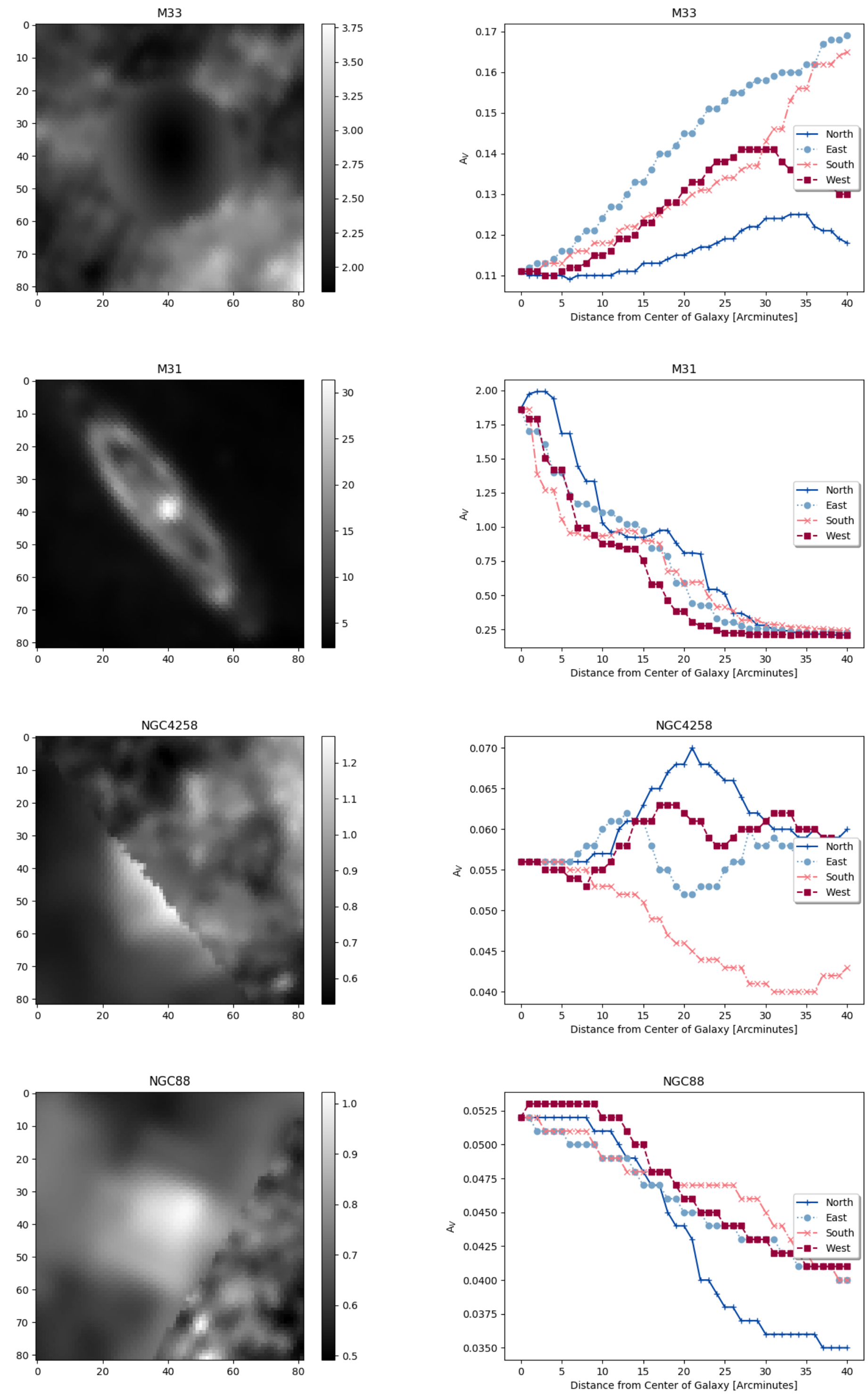

Figure 3. 100 μmIRAS images (80′× 80′with North pointing up) on the left and the corresponding plots of A_V versus distance from center for a few galaxies illustrating the range of contamination. In the first row, M33 has been oversubtracted, so the MW reddening would be underestimated. In the second panel, M31 has not been removed, with the recommended value from the appendix of SFD98 being reported by NED but not IRSA. The bottom panels show discontinuities in the reddening values near NGC4258 and NGC88 due to data gaps in the IRAS imaging.

REFERENCES

Astropy Collaboration, Robitaille, T. P., Tollerud, E. J., et al. 2013, A&A, 558, A33, doi: 10.1051/0004-6361/201322068

Brown, P. J., Breeveld, A. A., Holland, S., Kuin, P., & Pritchard, T. 2014, A&SS, 354, 89, doi: 10.1007/s10509-014-2059-8

Burstein, D., & Heiles, C. 1982, AJ, 87, 1165, doi: 10.1086/113199

Chiang, Y.-K., & Ménard, B. 2019, ApJ, 870, 120, doi: 10.3847/1538-4357/aaf4f6

Dalcanton, J. J., Williams, B. F., Seth, A. C., et al. 2009, ApJS, 183, 67, doi: 10.1088/0067-0049/183/1/67

Fitzpatrick, E. L. 1999, PASP, 111, 63, doi: 10.1086/316293

Foley, R. J., Fox, O. D., McCully, C., et al. 2014, MNRAS, 443, 2887, doi: 10.1093/mnras/stu1378

Ginsburg, A., Sipőcz, B. M., Brasseur, C. E., et al. 2019, AJ, 157, 98, doi: 10.3847/1538-3881/aafc33

Green, G. M., Schlafly, E., Zucker, C., Speagle, J. S., & Finkbeiner, D. 2019, ApJ, 887, 93, doi: 10.3847/1538-4357/ab5362

Haschke, R., Grebel, E. K., & Duffau, S. 2011, AJ, 141, 158, doi: 10.1088/0004-6256/141/5/158

Hoffmann, S. L., Macri, L. M., Riess, A. G., et al. 2016, ApJ, 830, 10, doi: 10.3847/0004-637X/830/1/10

Humphreys, E. M. L., Reid, M. J., Moran, J. M., Greenhill, L. J., & Argon, A. L. 2013, ApJ, 775, 13, doi: 10.1088/0004-637X/775/1/13

Johnson, L. C., Méndez, R. H., & Teodorescu, A. M. 2009, ApJ, 697, 1138, doi: 10.1088/0004-637X/697/2/1138

Jones, E., Oliphant, T., Peterson, P., et al. 2001–, SciPy: Open source scientific tools for Python. http://www.scipy.org/

Kennicutt, Robert C., J., Armus, L., Bendo, G., et al. 2003, PASP, 115, 928, doi: 10.1086/376941

Lenz, D., Hensley, B. S., & Doré, O. 2017, ApJ, 846, 38, doi: 10.3847/1538-4357/aa84af

Macri, L. M., Stanek, K. Z., Bersier, D., Greenhill, L. J., & Reid, M. J. 2006, ApJ, 652, 1133, doi: 10.1086/508530

Mazzarella, J. M., Madore, B. F., & Helou, G. 2001, in Proc. SPIE, Vol. 4477, Astronomical Data Analysis, ed. J.-L. Starck & F. D. Murtagh, 20–34, doi: 10.1117/12.447177

Phillips, M. M., Lira, P., Suntzeff, N. B., et al. 1999, AJ, 118, 1766, doi: 10.1086/301032

Planck Collaboration, Abergel, A., Ade, P. A. R., et al. 2014, A&A, 571, A11, doi: 10.1051/0004-6361/201323195

Price-Whelan, A. M., Sipőcz, B. M., Günther, H. M., et al. 2018, AJ, 156, 123, doi: 10.3847/1538-3881/aabc4f

Reid, M. J., Pesce, D. W., & Riess, A. G. 2019, ApJL, 886, L27, doi: 10.3847/2041-8213/ab552d

Rice, W., Lonsdale, C. J., Soifer, B. T., et al. 1988, ApJS, 68, 91, doi: 10.1086/191283

Riess, A. G., Macri, L. M., Hoffmann, S. L., et al. 2016, ApJ, 826, 56, doi: 10.3847/0004-637X/826/1/56

Schlafly, E. F., & Finkbeiner, D. P. 2011, ApJ, 737, 103, doi: 10.1088/0004-637X/737/2/103

Schlegel, D. J., Finkbeiner, D. P., & Davis, M. 1998, ApJ, 500, 525, doi: 10.1086/305772

Virtanen, P., Gommers, R., Oliphant, T. E., et al. 2020, Nature Methods, 17, 261, doi: 10.1038/s41592-019-0686-2

Table 1. Improved Estimates for the Galactic Extinction in the Line of Sight near External Galaxies in the Schlafly & Finkbeiner (2011) System

Galaxy Name	RA	Dec	Radius	A_V	Err[a]	Supernovae/Transients
	(H M S)	(D M S)	(arcmin)	(mag)	(mag)	
LMC	05h23m34.6s	-69d45m22s	323	0.20[b]	0.05	SN1987A
SMC	00h52m38.0s	-72d48m01s	190	0.10[b]	0.05	...
M31	00h42m44.5s	+41d16m09s	95	0.17[b]	0.05	SN1885A
M82	9h55m52.43s	69d40m46.93s	20	0.16[c]	0.05	SN2004am, SN2008iz, SN2014J, SN2019ajl
Arp244	12h01m53.17s	-18d52m37.92s	15	0.112	0.007	SNe 1921A, 1974E, 2004gt
Arp244	...	...	...	...	...	SNe 2007sr, 2013dk
ESO138-G10	16h59m02.952s	-60d12m57.67s	12	0.574	0.023	SN2013by
ESO287-G40	21h37m28.1842s	-47d02m08.8331s	7	0.067	0.004	SNe 2009lc, 2013fy
ESO317-32	10h28m01.6186s	-42d06m38.7541s	12	0.329	0.014	SN2017ghs
ESO509-IG064	13h34m39.3s	-23d40m50s	15	0.292	0.026	SN2016eiy
IC208	2h08m27.736s	6d23m41.53s	12	0.135	0.004	SNe 2003G, 2017glq
IC2574	10h28m23.6205s	68d24m43.4414s	15	0.094	0.010	...
IC5249	22h47m06.262s	-64d49m55.42s	15	0.087	0.004	SN2011cb
KUG0647+311	6h50m36.832s	31d07m00.6s	15	0.334	0.027	SN2016asf
M33	01h33m50.8900s	+30d39m36.800s	35	0.1445	0.011	SNe PS1-13dni, PS1-14ajo, PS1-14alm, PS1-14amp
M33	...	...	...	...	...	SNe PS15caq, PS15cab, PS15dfl, PS16yg
M33	...	...	...	...	...	SNe AT2016wf, AT2016fyi, AT2016uh, AT2019gc
M51	13h29m52.698s	47d11m42.93s	15	0.076	0.013	SNe 1945A, 1994I, 2005cs, 2011dh
M61	12h21m54.9275s	4d28m25.5883s	15	0.051	0.003	SNe 1926A, 1964F, 1961I, 1999gn
M61	...	...	...	...	...	SNe 2006ov, 2008in, 2014dt
M66	11h20m15.026s	12d59m28.64s	15	0.07	0.008	SNe 1973R, 1989B, 1997bs
M66	...	...	...	...	...	SNe 2009hd, 2016cok
M74	1h36m41.772s	15d47m00.46s	15	0.171	0.010	SNe 2002ap, 2003gd, 2013ej, PS15blm
M82	9h55m52.43s	69d40m46.93s	20	0.224	0.092	SNe 2004am, 2008iz, 2014J, 2019aji
M83	13h37m00.919s	-29d51m56.74s	15	0.127	0.011	SNe 1923A, 1945B, 1950B
M83	...	...	...	...	...	SNe 1957D, 1968L, 1983N
M106/NGC4258	12h18m57.5046s	+47d18m14.303	35	0.045	0.010	SNe SN1981K, PS1-11acn, PS1-13aea, SN2014bc

Table 1 *continued*

Table 1 *(continued)*

Galaxy Name	RA	Dec	Radius	A_V	Err[a]	Supernovae/Transients
	(H M S)	(D M S)	(arcmin)	(mag)	(mag)	
MCG-01-07-004	2h23m13.2516s	-4d31m01.5168s	7	0.071	0.002	SNe ASASSN-15od, SCP06R12, PS1-10g
MCG-02-24-027	9h28m59.256s	-14d48m27.25s	7	0.172	0.004	SN2011at
MCG-02-30-003	11h33m10.5799s	-10d13m43.7361s	10	0.095	0.003	SNe 2003ee, 2017hm
MCG+10-19-1	12h54m49.706s	58d52m56.46s	7	0.028	0.003	PTF10icb
NGC088	00h21m22.12s	-48d38m24.6s	30	0.046	0.005	SNe 1994Z, ASASSN-15ut
NGC0584	1h31m20.755s	-6d52m05.02s	15	0.102	0.006	SN2016fng
NGC1097	2h46m19.059s	-30d16m29.68s	15	0.054	0.003	SNe 1992bd, 1999eu, 2003B
NGC1313	3h18m16.046s	-66d29m53.74s	20	0.222	0.063	SNe 1962M, 1978K
NGC134	0h30m21.893s	-33d14m43.26s	20	0.03	0.004	SN2009gj
NGC1365	3h33m36.458s	-36d08m26.37s	20	0.034	0.004	SNe 1957C, 1983V, 2001du, 2012fr
NGC1371	3h35m01.351s	-24d55m59.19s	10	0.054	0.006	SN2005ke
NGC1448	3h44m31.915s	-44d38m41.38s	10	0.037	0.003	SNe 1983S, 2001el, 2003hn, 2014df
NGC2315	7h02m33.038s	50d35m26.18s	7	0.215	0.008	SN2011ay
NGC2357	7h17m40.981s	23d21m24.28s	10	0.164	0.014	SNe 2010bj, 2015I
NGC2577	8h22m43.45s	22d33m11.1408s	10	0.124	0.008	SN2007ax
NGC2615	8h34m33.358s	-2d32m48.57s	10	0.077	0.004	SN2014ao
NGC2668	8h49m22.57s	36d42m37.53s	10	0.088	0.003	SN2003je
NGC2748	9h13m43.037s	76d28m31.23s	5	0.071	0.005	SNe 1985A, 2013ff, PS15jf, 2017gkk
NGC2811	9h16m11.1s	-16d18m45.78s	12	0.123	0.005	SNe 2005am, 2018jzo
NGC3034	9h55m52.43s	69d40m46.93s	15	0.31	0.090	SNe 2004am, 2008iz, 2014J, 2019ajl
NGC3521	11h05m48.5676s	-0d02m09.2282s	15	0.121	0.018	...
NGC3556	11h11m30.967s	55d40m26.84s	20	0.029	0.008	SN1969B
NGC3627	11h20m15.026s	12d59m28.64s	15	0.07	0.008	SNe 1973R, 1989B, 1997bs, 2009hd, 2016cok
NGC3690	11h28m31.326s	58d33m41.8s	10	0.045	0.001	SNe 1992bu, 1993G, 1998T, 1999D
NGC3690	...	...	...	...	...	SNe 2005U, 2010O, 2010P, 2019lqo
NGC383	1h07m24.9587s	32d24m45.214s	14	0.162	0.007	SNe 2000dk, 2015ar, 2016sx, 2017hle
NGC3953	11h53m49.0088s	52d19m36.4738s	15	0.079	0.015	SNe 2001dp, 2006bp
NGC4080	12h04m51.804s	26d59m33.43s	12	0.055	0.002	MASTER OT J120451.50+265946.6
NGC4214	12h15m39.174s	36d19m36.8s	10	0.057	0.005	SNe 1954A, 2010U
NGC4569	12h36m49.816s	13d09m46.33s	7	0.125	0.008	...

Table 1 *continued*

Table 1 *(continued)*

Galaxy Name	RA	Dec	Radius	A_V	Err[a]	Supernovae/Transients
	(H M S)	(D M S)	(arcmin)	(mag)	(mag)	
NGC4594	12h39m59.4319s	-11d37m22.9954s	10	0.13	0.005	SNe 1997bl, PS15akv
NGC4631	12h42m08.009s	32d32m29.44s	10	0.046	0.003	...
NGC4736	12h50m53.148s	41d07m12.55s	15	0.039	0.006	...
NGC5055	13h15m49.2739s	42d01m45.7261s	15	0.0415	0.005	SN1971I
NGC5177	13h29m24.269s	11d47m49.55s	5	0.085	0.004	SN2010cr
NGC5221	13h34m55.909s	13d49m57.14s	10	0.068	0.003	SN1970P, SN2008ez, PS1-14ea, SN2016bln
NGC5490	14h09m57.33s	17d32m43.53s	10	0.066	0.003	SN1997cn, SN2003aq, SN2005I
NGC5490	...	...	...	...	...	SN2015bo, SN2016ccm
NGC613	1h34m18.235s	-29d25m06.56s	15	0.046	0.004	SN2016gkg
NGC6166	16h28m38.2444s	39d33m04.2318s	10	0.025	0.002	SN1997cq, SN2009eu, PS15aot
NGC6166	...	...	...	...	...	SN2018ccl, SN2019gqd
NGC634	1h38m18.679s	35d21m53.47s	10	0.12	0.003	SN2006Q, SN2008A
NGC6479	17h48m21.5875s	54d08m56.4765s	7	0.103	0.005	SN2007cl, SN2009ay
NGC6822	19h44m56.199s	-14d47m51.29s	20	0.551	0.045	...
NGC7187	22h02m44.4954s	-32d48m11.439s	10	0.085	0.003	SN2017gah
NGC7259	22h23m05.5451s	-28d57m17.4766s	7	0.045	0.002	SN2009ip, SN2014dq, SMT16jyu
NGC7371	22h46m03.744s	-11d00m04.3327s	7	0.145	0.005	LSQ13cux, PS15bgt
NGC7552	23h16m10.767s	-42d35m05.39s	12	0.035	0.004	SN2017bzc
NGC7653	23h24m49.3612s	15d16m32.1419s	7	0.177	0.009	SN2015bf, SN2018cjk
NGC7793	23h57m49.7534s	-32d35m27.7083s	12	0.041	0.004	SN2008bk
NGC88	0h21m22.132s	-48d38m24.28s	20	0.048	0.003	SN1994Z, ASASSN-15ut
NGC918	2h25m50.7911s	18d29m46.3842s	20	0.702	0.049	SN2009js, SN2011ek
PGC071943	23h37m44.414s	-47d30m22.92s	10	0.033	0.003	...
PGC2692384	18h32m24.016s	66d53m43s	15	0.16	0.02	SN2011hj
PGC29010	10h01m26.5223s	36d40m16.6648s	8	0.18	0.018	SN2012ak, PS15ahw
PGC68345	22h14m03.018s	-26d56m15.77s	10	0.033	0.004	SN2010bv, SN2016dgt
PGC83768	13h02m35.193s	27d26m21.38s	12	0.057	0.004	SN1962I, SN1991Q, SN2003do, SN2012da
PGC9204	2h25m28.346s	-25d38m16.46s	10	0.025	0.002	SN2014cp
SDSSJ161609.48+383245.0	16h16m09.485s	38d32m45.09s	7	0.034	0.001	SN2013eh
UGC09113	14h14m14.762s	35d25m23.83s	15	0.038	0.005	...

Table 1 *continued*

Table 1 *(continued)*

Galaxy Name	RA (H M S)	Dec (D M S)	Radius (arcmin)	A_V (mag)	Err[a] (mag)	Supernovae/Transients
UGC09386	14h34m52.7783s	40d44m52.8518s	15	0.047	0.009	SN2017daf
UGC10064	15h51m13.2752s	25d42m06.784s	13	0.173	0.008	SN2009dc, SN2019fee
UGC10214	16h06m03.94s	55d25m31.33s	5	0.023	0.001	SN2002lk, SN2007cu, SN2008dq
UGC10214	···	···	···	···	···	PS1-10acx, PS1-11agk
UGC10685	17h04m50.999s	12d55m29.64s	10	0.239	0.014	SN2010hw, SN2013cj
UGC11501	19h58m37.031s	2d36m10.62s	10	0.376	0.068	SN2011dn
UGC11797	21h43m20.1605s	43d34m34.644s	10	1.248	0.069	SN2004ca, SN2015N, SN2018dfy
UGC12640	23h30m56.799s	15d29m25.96s	10	0.169	0.008	SN2011ef, SN2019ssi
UGC12846	23h55m46.0248s	18d25m33.6036s	10	0.094	0.006	SN2007od
UGC12850	23h56m06.16s	29d22m40.44s	10	0.143	0.010	SN2014ek, CSSJ235535.6+291220
UGC2855	3h48m20.731s	70d07m58.37s	7	1.947	0.038	SN2014dg
UGC402	0h39m18.612s	3d57m08.87s	10	0.067	0.003	ASASSN-15qc, SN2016hsq
UGC4179	8h02m05.9609s	0d48m32.742s	5	0.147	0.019	SN2006jd
UGC5055	9h30m11.7493s	55d51m08.6863s	8	0.086	0.006	SN2014R
UGC5378	10h00m31.9918s	4d24m25.6711s	5	0.067	0.005	SN2007S
UGC5460	10h08m09.197s	51d50m40.2504s	5	0.022	0.003	SN2011ht, SN2015as
UGC5623	10h23m48.6038s	33d48m28.7892s	9	0.055	0.006	SN2010ks
UGC6483	11h29m02.358s	17d13m55.15s	7	0.069	0.003	SN2013hh
UGC7848	12h40m57.433s	63d31m11.3s	5	0.039	0.001	SN2006bv
UGC8713	13h47m01.2595s	33d53m36.9528s	10	0.054	0.004	SN2012cp

[a] This is the uncertainty on what the extinction would be from the Schlegel et al. (1998) maps converted to the Schlafly & Finkbeiner (2011) system. It does not include the overall 16% uncertainty of the maps themselves quoted by Schlegel et al. (1998) which should be added in quadrature.

[b] Value from Appendix C of Schlegel et al. (1998) converted to the Schlafly & Finkbeiner (2011) system.

[c] Value from Dalcanton et al. (2009) converted to the Schlafly & Finkbeiner (2011) system.